Available online at www.sciencedirect.com
ScienceDirect
Lithos 100 (2008) 93–111
LITHOS
www.elsevier.com/locate/lithos

Melting of the subcontinental lithospheric mantle by the Emeishan mantle plume; evidence from the basal alkaline basalts in Dongchuan, Yunnan, Southwestern China

Xie-Yan Song [a,*], Hua-Wen Qi [a], Paul T. Robinson [b], Mei-Fu Zhou [c], Zhi-Min Cao [d], Lie-Meng Chen [a]

[a] *State Key Laboratory of Ore Deposit Geochemistry, Institute of Geochemistry, Chinese Academy of Sciences, 46 Guanshui Road, Guiyang, 550002, PR China*
[b] *Department of Earth Sciences, Dalhousie University, Halifax, Nova Scotia, Canada B3H 4J1*
[c] *Department of Earth Sciences, The University of Hong Kong, Hong Kong, PR China*
[d] *College of Earth Sciences, Ocean University of China, Qingdao, PR China*

Received 7 August 2006; accepted 8 June 2007
Available online 3 August 2007

Abstract

The Emeishan continental flood basalt (ECFB) sequence in Dongchuan, SW China comprises a basal tephrite unit overlain by an upper tholeiitic basalt unit. The upper basalts have high TiO_2 contents (3.2–5.2 wt.%), relatively high rare-earth element (REE) concentrations (40 to 60 ppm La, 12.5 to 16.5 ppm Sm, and 3 to 4 ppm Yb), moderate Zr/Nb and Nb/La ratios (9.3–10.2 and 0.6–0.9, respectively) and relatively high $\varepsilon_{Nd\ (t)}$ values, ranging from −0.94 to 2.3, and are comparable to the high-Ti ECFB elsewhere. The tephrites have relatively high P_2O_5 (1.3–2.0 wt.%), low REE concentrations (e.g., 17 to 23 ppm La, 4 to 5.3 ppm Sm, and 2 to 3 ppm Yb), high Nb/La (2.0–3.9) ratios, low Zr/Nb ratios (2.3–4.2), and extremely low $\varepsilon_{Nd\ (t)}$ values (mostly ranging from −10.6 to −11.1). The distinct compositional differences between the tephrites and the overlying tholeiitic basalts cannot be explained by either fractional crystallization or crustal contamination of a common parental magma. The tholeiitic basalts formed by partial melting of the Emeishan plume head at a depth where garnet was stable, perhaps >80 km. We propose that the tephrites were derived from magmas formed when the base of the previously metasomatized, volatile-mineral bearing subcontinental lithospheric mantle was heated by the upwelling mantle plume.

Keywords: Emeishan flood basalts; Tephrite; Metasomatized subcontinental lithospheric mantle; Partial melting; Mantle plume

1. Introduction

The geochemistry of continental flood basalts can yield valuable information about the nature of the mantle sources from which they were derived and about the extent of plume–lithosphere interaction. The voluminous lavas in typical flood basalt provinces are generally considered to reflect asthenospheric melting

* Corresponding author. State Key Laboratory of Ore Deposit Geochemistry Institute of Geochemistry, Chinese Academy of Sciences 46 Guanshui Road, Guiyang, 550002, PR China. Tel./fax: +86 851 5895538.
E-mail address: songxieyan@vip.gyig.ac.cn (X.-Y. Song).

0024-4937/$ - see front matter © 2007 Published by Elsevier B.V.
doi:10.1016/j.lithos.2007.06.023

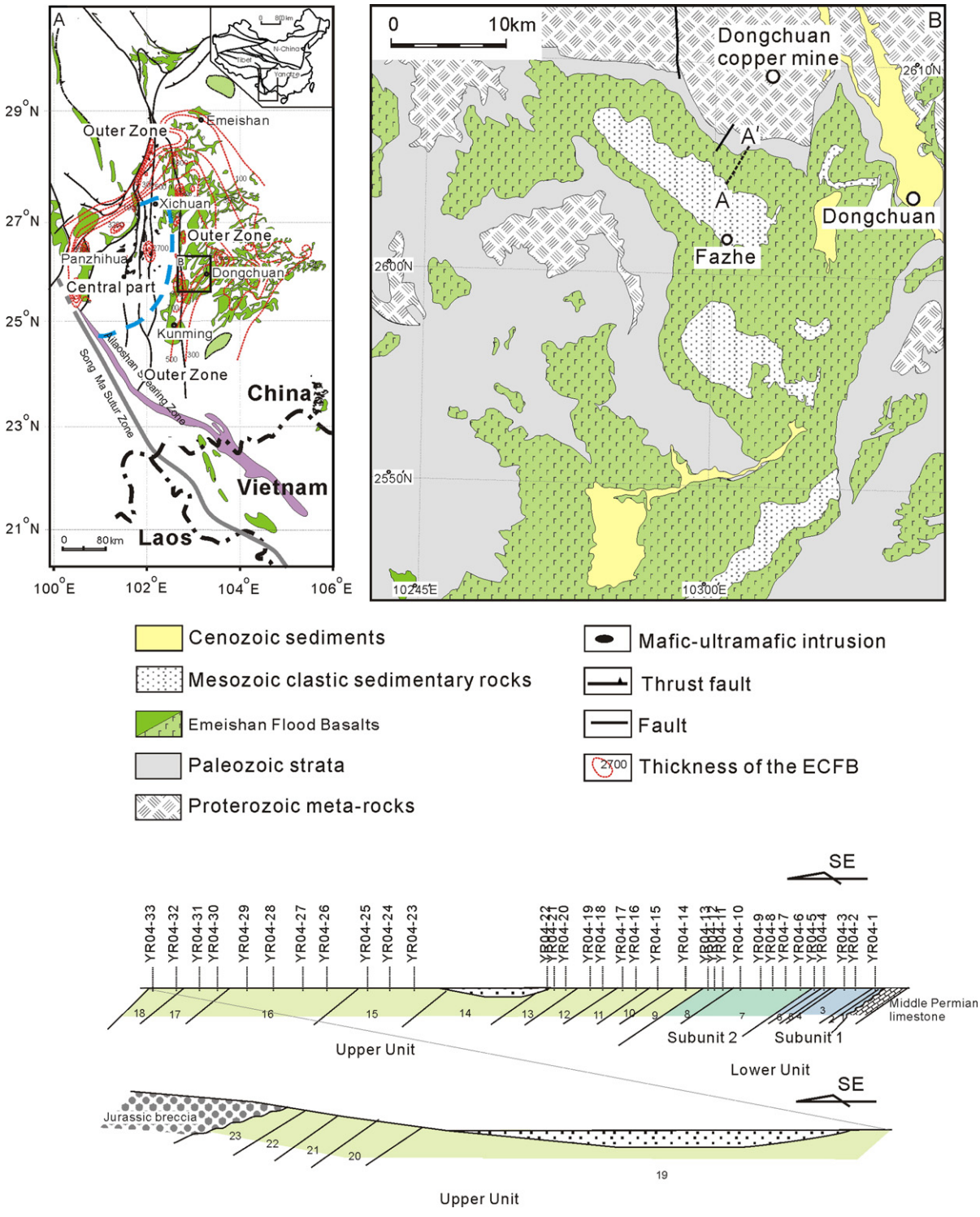

Fig. 1. Distribution of the Emeishan continental flood basalts and related intrusions in the Emeishan large igneous province (A), in the Dongchuan area (B), and (C) cross-section of the ECFB in Dongchuan.

and decompressional melting of the associated mantle plume, whereas small volumes of lithospheric mantle-derived magmas may be generated when the lithosphere is heated by the mantle plume (e.g. McKenzie and Bickle, 1988; White and McKenzie, 1989; Arndt and Christensen, 1992). However, other authors have argued that a large proportion of the lavas may have originated from metasomatically enriched subcontinental lithospheric mantle (SCLM) (e.g. Gallagher and Hawkesworth, 1992; Turner et al., 1996).

The ECFB, which consist dominantly of tholeiitic basalts, cover an area over 5×10^5 km^2 in southwest China and northern Vietnam, and have been studied extensively over the last decade (e.g. Chung and Jahn, 1995; Song et al., 1998, 2001, 2004; Thompson et al., 2001; Xu et al., 2001; Zhou et al., 2002a,b; Ali et al., 2002, 2005). They are generally interpreted as the products of a Middle/Late Permian mantle plume contaminated by the SCLM beneath the Emeishan large igneous province (ELIP) (Song et al., 2001; Xiao et al., 2003) or mixed with lamproitic magmas from the SCLM (Chung and Jahn, 1995). However, the nature of the SCLM beneath the ELIP is not well constrained, and the degree of melting of the SCLM, if any, during plume activity is not clear.

For the first time, we describe alkaline lavas associated with the ECFB in a cross-section at Dongchuan, Yunnan Province, SW China. New geochemical and Sr–Nd isotopic data on the alkaline and tholeiitic basalts from Dongchuan (Fig. 1) are used to investigate the relative contributions of SCLM and mantle plume melts to the ECFB and to determine the compositional nature of the SCLM source beneath the ELIP. These new data suggest that the alkaline basalts in the Dongchuan area formed by partial melting of metasomatised domains at the base of the SCLM, whereas the overlying tholeiitic basalts were derived dominantly by decompressional melting of the mantle plume.

2. Geological background

The Yangtze craton of southern China consists of a Proterozoic crystalline basement uncomfortably overlain by Sinian to Middle Permian marine clastic rocks and carbonates. The Middle/Late Permian ECFB overlies Middle Permian limestone and is unconformably overlain by Late Permian–Cretaceous terrestrial clastic sedimentary rocks (GMBY, 1978; GMBS, 1991). Mafic–ultramafic intrusions associated with the ECFB have been dated at 260 Ma (Fig. 1) (Zhou et al., 2002).

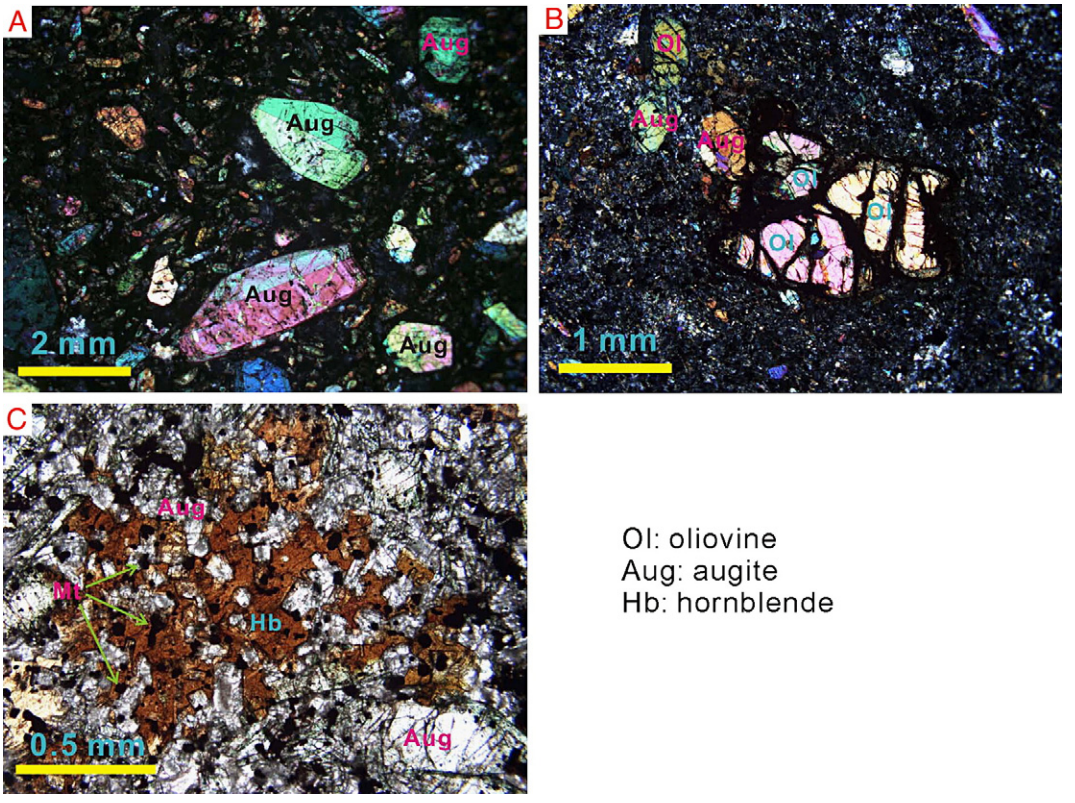

Fig. 2. Photos showing phenocrysts of clinopyroxene (A) and olivine (B) and interstitial hornblende crystal (C) in the tephrites.

Table 1
Concentrations of major and trace elements of the Dongchuan ECFB

Lower Unit (tephrite)													
	YR04-1	YR04-2	YR04-3	YR04-4	YR04-5	YR04-6	YR04-7	YR04-8	YR04-9	YR04-10	YR04-11	YR04-12	YR04-13
Major oxides (wt.%)													
SiO_2	40.4	43.1	42.7	41.8	39.7	41.7	43.9	43.3	42.6	42.0	43.3	42.9	44.1
TiO_2	1.7	2.1	2.0	1.9	2.0	1.9	1.9	1.9	1.9	1.9	1.9	2.0	1.9
Al_2O_3	11.3	11.8	11.0	11.1	12.0	7.0	12.9	12.9	11.8	12.5	13.2	12.4	13.9
Fe_2O_3	12.4	14.0	14.1	12.8	13.0	13.8	12.7	12.5	12.8	12.7	12.5	12.8	12.7
MnO	0.3	0.3	0.2	0.2	0.3	0.4	0.2	0.2	0.2	0.2	0.2	0.2	0.2
MgO	7.5	6.8	7.0	7.5	6.5	11.5	5.7	5.7	6.2	5.7	5.5	6.0	5.5
CaO	12.9	12.1	11.9	11.9	13.8	16.3	10.2	9.8	11.9	10.0	10.1	10.7	10.7
Na_2O	4.1	2.5	3.0	3.9	3.4	1.8	4.4	5.6	3.7	5.2	4.9	4.9	3.2
K_2O	0.7	3.0	2.2	0.8	0.8	0.6	2.5	2.3	2.9	2.2	2.1	1.8	2.7
P_2O_5	1.4	1.3	1.4	1.9	1.6	1.4	1.4	1.5	1.5	1.5	1.5	1.5	1.4
LOI	7.0	4.8	4.8	5.8	6.5	3.8	3.7	3.1	4.0	4.2	4.4	4.2	4.0
Total	99.7	101.8	100.3	99.6	99.6	100.2	99.5	98.8	99.5	98.1	99.6	99.4	100.3
Trace elements (ppm)													
Sc	20.2	22.4	22.9	25.6	19.6	41.7	18.4	18.9	19.3	18.8	18.4	20.5	18.9
V	350	489	259	296	470	353	342	310	314	339	367	368	354
Cr	29.2	29.2	28.5	42.5	35.5	261.3	17.2	26.9	17.0	16.6	14.8	20.2	24.7
Co	42.4	48.2	51.3	46.5	47.0	55.2	42.9	42.2	43.6	44.2	40.8	43.6	41.7
Ni	23.2	28.4	32.1	32.1	30.0	73.6	18.8	20.6	19.9	20.7	20.2	21.7	21.0
La	17.0	20.5	19.9	18.6	15.2	18.8	22.3	21.5	22.9	21.5	22.5	22.8	22.1
Ce	31.4	36.2	34.9	33.3	27.0	33.6	40.5	39.7	41.5	40.3	41.5	42.2	40.4
Pr	4.04	4.64	4.45	4.32	3.58	4.31	5.20	5.03	5.30	5.02	5.25	5.38	5.14
Nd	16.9	19.0	18.3	17.7	15.5	17.6	21.2	20.4	21.8	21.0	21.5	22.3	20.5
Sm	4.34	4.88	4.58	4.47	4.42	4.18	5.07	4.90	5.19	4.99	5.12	5.33	4.86
Eu	1.26	1.36	1.85	1.25	1.29	1.22	1.63	1.48	1.88	1.55	1.53	1.60	1.50
Gd	4.11	4.58	4.72	4.29	4.62	3.92	4.72	4.51	5.21	4.60	4.49	4.89	4.44
Tb	0.675	0.727	0.703	0.686	0.762	0.609	0.713	0.679	0.727	0.697	0.704	0.726	0.696
Dy	4.13	4.44	4.34	4.13	4.90	3.69	4.31	4.18	4.40	4.20	4.35	4.36	4.10
Ho	0.800	0.883	0.822	0.797	0.975	0.703	0.844	0.824	0.851	0.797	0.827	0.859	0.828
Er	2.32	2.55	2.41	2.27	2.85	2.07	2.45	2.38	2.46	2.39	2.42	2.52	2.40
Tm	0.365	0.411	0.384	0.370	0.463	0.333	0.396	0.381	0.390	0.377	0.385	0.398	0.382
Yb	2.31	2.57	2.37	2.23	2.89	2.02	2.52	2.38	2.54	2.40	2.48	2.58	2.41
Lu	0.341	0.364	0.332	0.315	0.411	0.297	0.371	0.354	0.366	0.346	0.365	0.369	0.355
Rb	22.2	98.0	87.1	14.6	32.7	16.9	71.3	69.3	93.7	77.1	82.3	93.1	50.9
Sr	899	454	584	688	600	497	714	554	562	577	657	370	541
Ba	867	704	3653	662	632	382	894	708	2402	815	825	765	672
Y	21.6	24.3	22.0	21.4	26.9	19.1	22.6	22.0	22.7	21.9	22.6	23.2	21.8
Nb	61.0	81.9	76.7	65.7	55.5	56.4	46.5	47.7	48.0	47.1	51.2	46.9	48.1
Ta	3.14	4.31	4.09	3.74	2.93	3.06	2.67	2.96	2.75	2.85	3.97	2.65	2.71
Zr	125	182	166	136	123	130	195	178	195	180	195	188	180
Hf	3.19	4.77	4.45	4.02	3.28	3.70	4.64	4.59	4.59	4.33	4.63	4.68	4.57
Th	4.93	6.44	6.80	5.87	3.78	4.11	4.63	4.43	4.57	4.06	4.60	4.45	4.45
U	1.20	0.98	0.83	1.15	1.84	0.61	1.09	1.23	1.25	1.11	1.17	1.26	1.25
Pb	6.13	11.06	16.15	13.58	11.66	7.29	12.69	12.36	12.55	12.16	11.24	11.62	11.53
Ratios													
Ta/La	0.18	0.21	0.21	0.20	0.19	0.16	0.12	0.14	0.12	0.13	0.18	0.12	0.12
Zr/Nb	2.1	2.2	2.2	2.1	2.2	2.3	4.2	3.7	4.1	3.8	3.8	4.0	3.7

The ELIP can be divided into a central part and an outer zone (Song et al., 2005a,b) (Fig. 1). Extensive erosion and thinning of the Middle Permian limestone in the central part of the ELIP indicates kilometer-scale regional uplift linked to the rising plume prior to eruption of the ECFB (He et al., 2003; Xu et al., 2004). The central part is characterized by low-Ti basalts overlain by high-Ti basalts, the presence of large layered intrusions hosting

Upper Unit (alkaline and tholeiitic lavas)										
YR04-14	YR04-15	YR04-16	YR04-17	YR04-18	YR04-19	YR04-20	YR04-21	YR04-22	YR04-23	YR04-24
Major oxides (wt.%)										
48.8	51.9	49.3	48.6	52.0	51.6	51.8	51.7	47.3	51.3	48.3
3.8	3.5	4.2	4.2	3.5	3.8	3.8	3.8	4.3	3.5	4.2
13.6	13.5	13.4	13.2	13.1	12.6	12.6	12.6	13.3	13.3	13.1
13.4	13.1	13.7	13.6	12.6	13.8	13.9	14.1	14.6	13.7	13.9
0.2	0.2	0.1	0.2	0.2	0.2	0.2	0.2	0.2	0.2	0.2
4.9	4.1	4.5	4.4	3.8	3.3	3.2	3.4	4.0	3.9	4.5
6.5	7.8	9.0	9.0	8.3	8.1	8.3	8.1	8.1	8.7	9.2
3.8	2.0	2.4	2.1	2.1	2.0	2.1	2.1	2.4	2.3	2.0
0.9	2.0	1.3	1.6	1.4	1.6	1.6	1.4	2.3	1.2	1.4
0.4	0.4	0.4	0.4	0.4	0.5	0.5	0.5	0.5	0.4	0.4
3.1	1.8	1.5	2.6	1.8	1.9	1.8	2.0	2.8	2.0	2.8
99.4	100.3	99.8	99.9	99.2	99.4	99.8	99.9	99.8	100.5	100.0
Trace elements (ppm)										
25.9	25.7	24.5	26.5	26.1	23.5	23.6	23.7	25.7	25.6	26.5
419	385	440	463	387	416	420	413	461	382	461
65.4	31.5	51.2	74.6	33.2	10.7	5.6	10.1	22.3	31.9	73.1
43.1	38.3	41.5	42.0	38.4	39.9	37.6	39.4	45.3	38.6	41.7
77.2	37.2	69.1	69.2	39.0	31.6	28.9	32.4	59.2	39.1	68.2
47.4	47.1	49.9	49.1	47.1	54.3	58.2	58.3	54.1	52.6	49.8
102.7	109.2	108.8	106.1	111.1	127.2	133.0	128.5	122.8	110.5	103.9
13.5	14.2	14.7	13.9	14.3	16.8	17.1	16.9	16.4	14.2	13.6
56.0	58.6	60.8	59.8	59.6	70.3	72.1	71.1	69.3	58.8	56.5
12.7	13.0	13.7	13.5	13.0	15.8	16.4	16.1	15.4	13.2	12.9
3.18	3.10	3.53	3.37	3.11	3.88	3.99	3.81	3.72	3.08	3.28
10.14	10.61	10.96	10.95	10.94	12.77	13.23	13.20	12.44	10.69	10.60
1.469	1.521	1.522	1.508	1.517	1.782	1.834	1.839	1.755	1.513	1.487
8.15	8.28	8.09	7.99	8.25	9.63	9.71	9.77	9.41	8.33	7.88
1.446	1.455	1.401	1.404	1.462	1.653	1.680	1.678	1.651	1.483	1.395
3.87	3.93	3.72	3.68	4.02	4.36	4.39	4.40	4.34	3.98	3.69
0.585	0.575	0.532	0.532	0.583	0.631	0.645	0.631	0.622	0.582	0.516
3.46	3.41	3.08	3.08	3.40	3.78	3.82	3.66	3.68	3.48	3.08
0.496	0.479	0.425	0.427	0.488	0.499	0.506	0.496	0.488	0.477	0.415
20.3	48.8	28.1	47.9	34.3	57.9	51.6	30.4	68.3	37.2	52.3
583	418	628	619	468	564	589	587	513	497	492
683	446	531	454	502	505	538	506	513	488	352
36.9	37.8	36.1	36.3	38.0	42.2	43.5	42.5	41.3	37.6	35.4
39.8	38.8	44.2	43.9	39.2	47.2	48.1	47.8	47.3	38.8	43.0
2.86	2.85	3.16	3.13	2.86	3.52	3.69	3.54	3.65	2.86	3.14
370	393	415	413	395	474	478	478	467	393	398
8.49	8.82	9.06	9.11	8.79	10.70	10.71	10.65	10.37	8.86	8.89
7.57	9.43	6.89	6.48	9.46	9.84	10.1	9.81	9.80	9.69	6.46
1.51	2.12	1.61	1.53	2.12	2.35	2.51	2.46	2.40	2.14	1.41
6.83	7.67	9.27	5.73	7.82	7.22	8.71	7.97	9.94	7.07	6.30
Ratios										
0.06	0.06	0.06	0.06	0.06	0.06	0.06	0.06	0.07	0.05	0.06
9.3	10.1	9.4	9.4	10.1	10.0	9.9	10.0	9.9	10.1	9.3

(continued on next page)

giant V–Ti-magnetite deposits and numerous syenite and alkaline granite plutons, whereas the outer zone consists of high-Ti basalts (e.g. Zhang and Luo, 1988; Song et al., 2005a,b, 2006). The ECFB volcanic sequence generally decreases in thickness from the central part of the ELIP to the edge (Xu et al., 2004; Song et al., 2004).

In the Dongchuan region, near the central ELIP (Fig. 1A and B), the ECFB is divided into a Lower Unit

Table 1 (*continued*)

	Upper Unit (alkaline and tholeiitic lavas)								
	YR04-25	YR04-26	YR04-27	YR04-28	YR04-29	YR04-30	YR04-31	YR04-32	YR04-33
Major oxides (wt.%)									
SiO_2	47.5	50.7	50.1	46.6	50.2	49.2	47.8	44.7	46.6
TiO_2	4.4	3.6	3.5	3.9	4.2	3.9	4.3	4.6	4.9
Al_2O_3	14.3	13.5	13.7	13.6	13.0	13.0	12.4	13.4	14.0
Fe_2O_3	14.5	13.1	12.9	14.8	13.9	13.8	15.4	14.8	14.3
MnO	0.2	0.2	0.2	0.2	0.2	0.2	0.2	0.2	0.3
MgO	5.1	4.0	4.1	4.6	3.7	4.4	4.8	5.8	5.5
CaO	7.5	8.5	7.9	8.9	8.6	9.2	9.7	7.7	4.7
Na_2O	3.7	2.0	1.9	2.3	2.1	1.9	2.0	3.3	3.5
K_2O	1.4	1.7	2.1	2.0	1.4	1.1	0.8	0.7	0.2
P_2O_5	0.5	0.4	0.4	0.4	0.5	0.4	0.4	0.4	0.3
LOI	0.9	2.2	2.6	2.8	2.0	2.2	2.0	3.6	5.9
Total	100.0	99.9	99.4	100.1	99.8	99.3	99.8	99.2	100.2
Trace elements (ppm)									
Sc	27.1	26.2	26.1	28.6	25.2	27.6	27.2	29.7	31.6
V	473	390	389	497	450	464	472	519	499
Cr	75.8	42.8	35.4	62.8	22.1	59.5	60.9	62.1	63.5
Co	41.9	40.4	38.1	44.4	41.5	45.2	45.7	48.3	50.7
Ni	67.4	41.3	40.2	57.9	47.1	65.1	71.2	64.3	65.3
La	52.7	53.6	57.0	41.3	56.5	44.6	44.6	45.9	51.2
Ce	109.0	109.5	112.2	89.2	118.8	91.0	91.2	97.4	109.5
Pr	14.2	14.2	14.7	12.1	15.8	12.6	12.7	13.2	14.8
Nd	59.2	58.5	59.4	52.7	65.6	53.4	54.2	55.7	63.2
Sm	13.5	13.1	13.2	12.6	14.8	13.1	13.3	13.4	14.5
Eu	3.38	2.98	3.21	3.18	3.56	3.22	3.26	3.40	3.49
Gd	11.03	10.62	11.24	10.73	12.19	10.51	11.07	11.64	11.72
Tb	1.545	1.517	1.564	1.518	1.701	1.544	1.590	1.695	1.662
Dy	8.31	8.22	8.54	8.38	9.14	8.43	8.83	9.02	8.91
Ho	1.443	1.473	1.506	1.467	1.593	1.486	1.475	1.567	1.569
Er	3.80	3.97	4.09	3.96	4.11	3.90	3.86	4.11	4.11
Tm	0.539	0.567	0.577	0.554	0.604	0.558	0.559	0.595	0.575
Yb	3.22	3.35	3.47	3.28	3.49	3.24	3.28	3.59	3.31
Lu	0.427	0.473	0.490	0.454	0.484	0.445	0.441	0.475	0.470
Rb	46.8	42.1	75.3	86.0	29.3	39.5	16.7	25.5	8.6
Sr	670	417	557	484	540	481	502	471	358
Ba	453	465	639	312	453	282	381	258	38
Y	35.6	38.2	38.3	37.9	39.9	36.8	38.9	38.8	40.9
Nb	44.4	39.5	39.9	36.1	45.0	36.4	39.6	41.7	44.3
Ta	3.28	3.04	3.22	2.62	3.33	2.88	2.99	3.32	3.29
Zr	413	397	399	364	445	371	378	402	423
Hf	8.92	8.86	9.00	8.34	9.96	8.53	8.45	8.53	9.31
Th	6.39	9.35	9.84	6.31	9.07	6.76	6.13	6.21	6.76
U	1.49	2.09	2.16	1.54	2.25	1.56	1.48	1.50	1.52
Pb	6.46	8.23	8.37	6.73	8.09	6.86	5.35	5.74	5.61
Ratios									
Ta/La	0.06	0.06	0.06	0.06	0.06	0.06	0.07	0.07	0.06
Zr/Nb	9.3	10.1	10.0	10.1	9.9	10.2	9.5	9.6	9.6

consisting dominantly of tephrites and an Upper Unit consisting of tholeiitic basalt. The Lower Unit rests uncomfortably on Middle Permian limestone and consists of 8 lava flows with an aggregate thickness of about 250 m. Individual flows range from 5 to 70 m thick, and are typically porphyritic at the base and amygdaloidal at the top (Fig. 1). Some are separated by thin layers of volcaniclastic material.

The tephrite flows are fresh to weakly or moderately altered and contain variable proportions of augite, nepheline, hornblende and olivine phenocrysts set in a fine-grained groundmass composed of augite, nepheline, aphanitic material and sparse Fe-oxides. Stubby prisms of augite, up to 1 cm in size, are the most common phenocryst phase (Fig. 2A), and many are compositionally zoned, increasing in Na_2O, FeO and TiO_2 from core to rim (unpublished data). Olivine phenocrysts ($Fo_{78–82}$) are small and sparse (Fig. 2B). Large, irregular phenocrysts of hornblende are scattered through the rock, and many contain minute crystals of augite, nepheline and Fe–Ti oxides along their margins and in fractures (Fig. 2C). Because the hornblende occurs only as a phenocryst phase, rather than rimming or replacing pyroxene, it is considered to be primary in origin. Nepheline phenocrysts occur only in the upper lava flows, where they are locally altered to analcime.

The Upper Unit conformably overlies the Lower Unit lavas, ranges from about 500 to 1000 m thick, and consists predominately of weakly altered tholeiitic basalt. More than 10 flows have been identified in this sequence (BGMY, 1978). Individual flows are typically massive and porphyritic at the base and amygdaloidal at the top, and the proportion of amygdaloidal lava increases upward in the section. Plagioclase is the only common phenocryst in these lavas, although it may be accompanied locally by minor augite. The groundmass of the tholeiitic basalts consists of fine-grained plagioclase, augite and minor Fe–Ti oxides.

The lavas of the Lower Unit are slightly more altered than those of the Upper Unit (see section 4.1) but, except for nepheline, most of the phenocryst phases in the tephrites are relatively fresh. Although the contact between the two units is not well exposed, the lavas are conformable and no paleo-soil or erosional surface has been observed at the boundary. Thus, we conclude that the difference in age of the two units is small.

3. Analytical techniques

Only the freshest, massive portions of individual flows were selected for chemical analysis, and the samples were ground in an agate mill. Major oxides were determined by X-ray fluorescence spectrometry (XRF) on fused glass pellets at the Institute of Geochemistry, Chinese Academy of Sciences. Trace elements, including REE, were analyzed by Inductively Coupled Plasma Mass Spectrometry (ICP-MS) at Nanjing University. We used standard additions, pure elemental standards for external calibration, and BHVO-1 as a reference material. Accuracy and precision of the XRF analyses are estimated to be 2% for major oxides present in concentrations greater than 0.5 wt.% and 5%

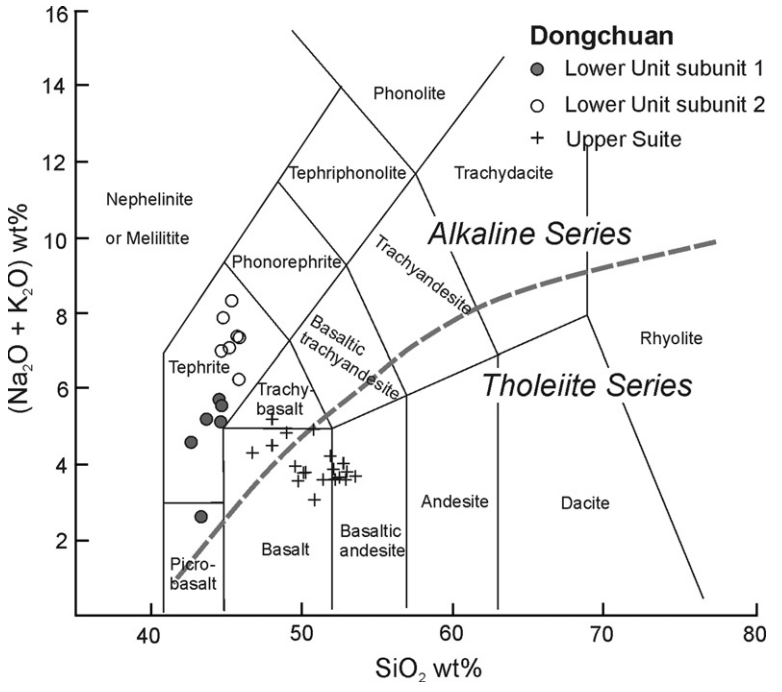

Fig. 3. Total alkalis vs silicate (TAS) diagram for volcanic rocks after Le Maitre et al. (1989). The subdivision of alkaline and tholeiitic after Irvine and Baragar (1971).

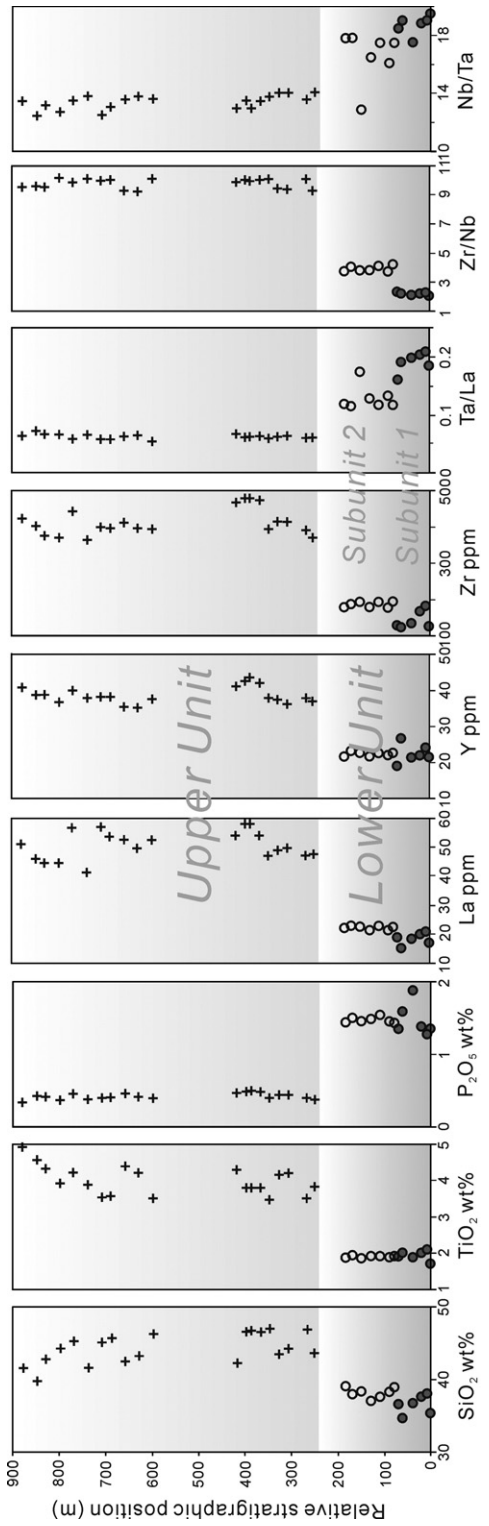

Fig. 4. Chemostratigraphic columns of the Dongchuan lava sequence.

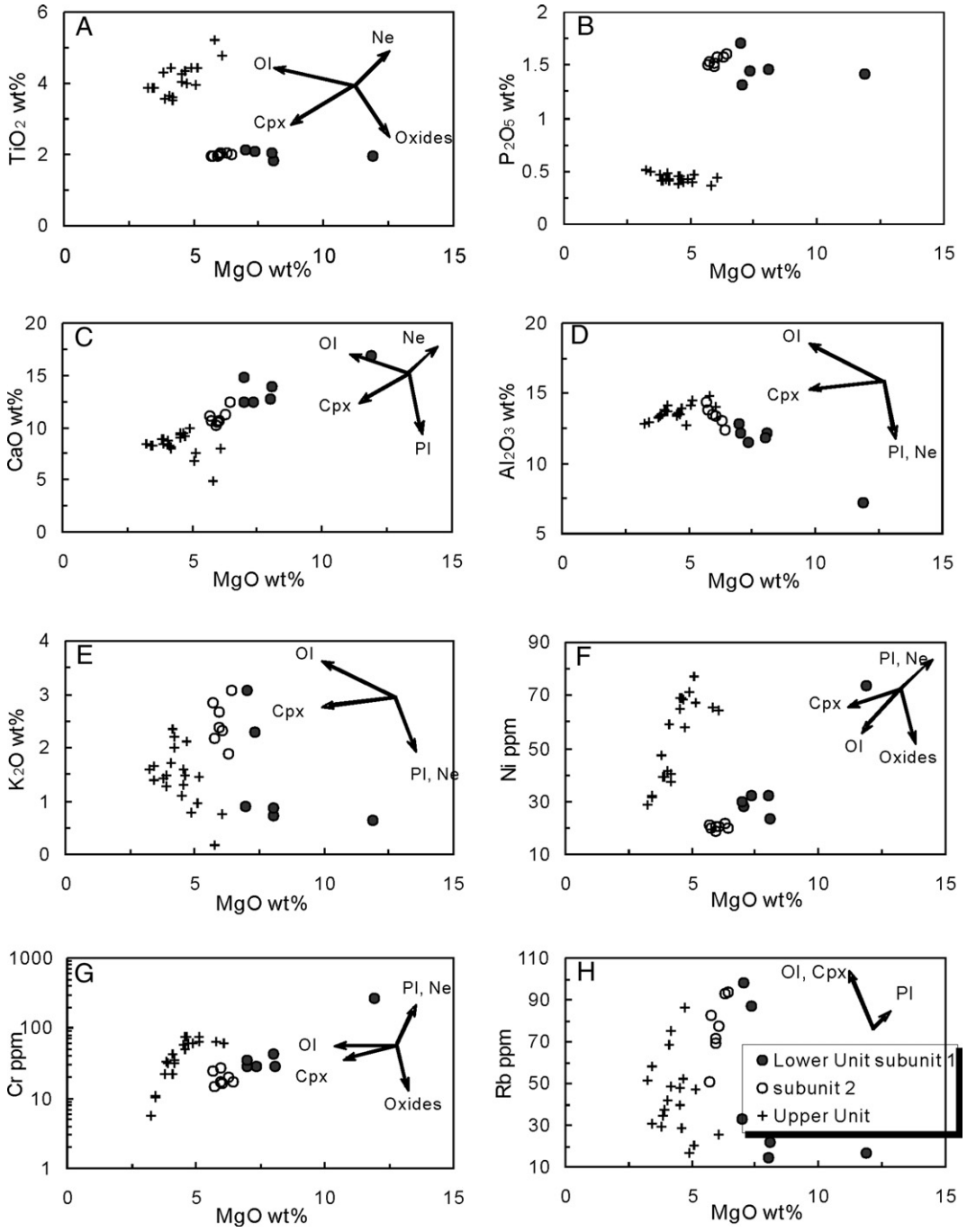

Fig. 5. Variation diagrams of major and trace elements against MgO for the Dongchuan lavas. Ol: olivine, Cpx: clinopyroxene, Pl: plagioclase, Ne: nepheline.

for trace elements. Accuracy and precision of the ICP-MS analyses are better than 5% (Zhou et al., 2000).

For Sm–Nd isotopic analyses, sample powders were spiked with mixed isotope tracers, dissolved in Teflon capsules with $HF+HNO_3$ acid, and separated by conventional cation-exchange techniques. Isotopic measurements were performed on the VG-354 mass-spectrometer at the Institute of Geology and Geophysics, Chinese Academy of Sciences. The mass fractionation corrections for Sr and Nd isotopic ratios were based on $^{86}Sr/^{88}Sr=0.1194$ and $^{146}Nd/^{144}Nd=0.7219$. Detailed sample preparation and analytical procedures followed Zhang et al. (2001).

4. Bulk-rock geochemistry

4.1. Influence of alteration on chemical composition

The tephrites of the lower unit were variably altered and metamorphosed following their eruption and burial. Secondary minerals, such as analcime and chlorite, commonly replace nepheline and augite phenocrysts, respectively. Loss on ignition (LOI) for the tephrites ranges from 3.1 to 7.0 and averages 4.6 wt.% (Table 1). Among the major oxides, normalized values of Al_2O_3 and P_2O_5 do not vary with LOI, whereas CaO, TiO_2, Fe_2O_3 and MgO increase slightly, and SiO_2 decreases, with increasing LOI. Mobile elements, such as Rb, Sr, K, Ca, and Ba, show moderate degrees of scatter.

The upper tholeiitic basalts are generally fresher than the tephrites and are characterized by the deposition of chlorite, calcite, and opal in amygdules. LOI for these lavas ranges from 0.9 to 5.9 and averages 2.4 wt.%. Normalized values of TiO_2, Fe_2O_3 and P_2O_5 show no variation with LOI, whereas Al_2O_3 and MgO increase, and SiO_2 decreases, with increasing LOI. CaO generally correlates positively with LOI except for sample YR04–33, which has the highest LOI and is strongly depleted in CaO. Again, mobile elements show variable degrees of scatter, thus in the following discussion, we focus on REE and high field strength elements (HFSE), Nb, Ta, Y, Al, P, and Ti (cf., Arndt et al., 1998).

4.2. Major oxides and transition metals

The major oxide concentrations of the Dongchuan lavas are listed in Table 1. The values shown in Figs. 3, 4 and 5 have been recalculated to 100% on an anhydrous basis, and these are the values discussed below.

Tephrites of the Lower Unit are characterized by low SiO_2 (42.6–45.86 wt.%), high total alkalis (2.5–8.3 wt.%) (Fig. 3), extremely high P_2O_5 (1.3–2.0 wt.%), and relatively low TiO_2 (1.8 to 2.2 wt.%) (Figs. 4 and 5). In contrast, the Upper Unit lavas have relatively high SiO_2 (46.0 to 53.4 wt.%), generally low total alkalis (2.9–5.1 wt.%) (Fig. 3), much lower P_2O_5 (0.32–0.52 wt.%) and higher TiO_2 (3.2–5.2 wt.%) (Figs. 4 and 5). Although the Lower Unit lavas have higher MgO contents (5.48 to 11.5 wt.%) than the Upper Unit lavas (3.18 to 5.8 wt.%) (Fig. 5), the Ni concentrations of the former (18 to 33 ppm, except for sample YR04–6) are generally lower than those of the latter (40–77 ppm) (Table 1).

The different groups also show distinct trends on MgO variation diagrams. In the lower lavas, TiO_2 remains

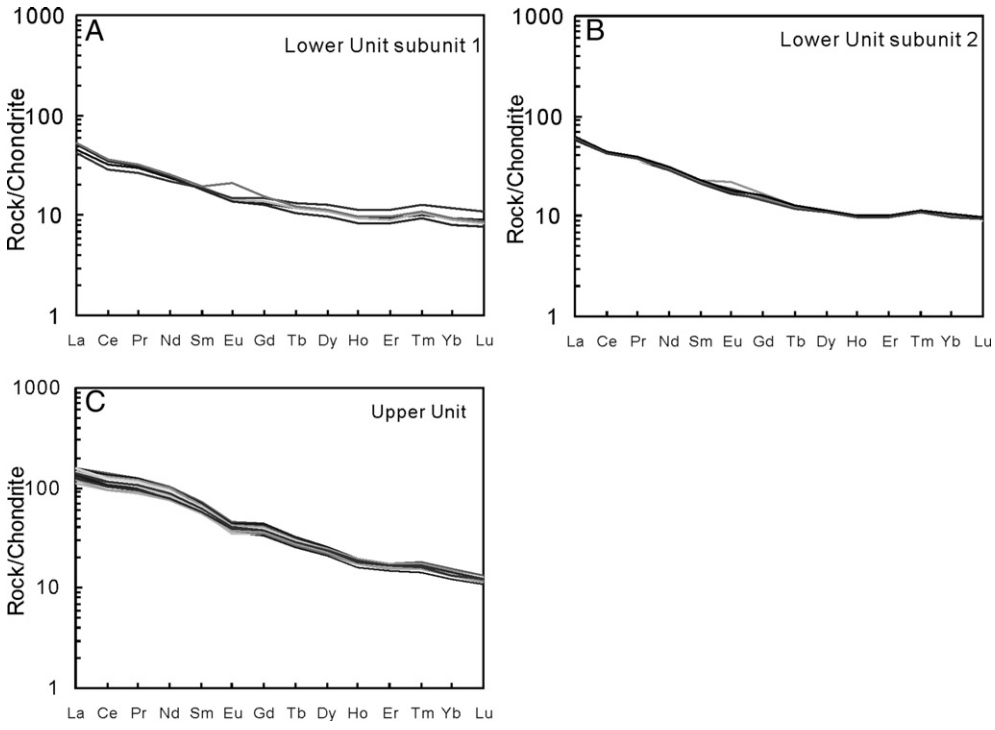

Fig. 6. Chondrite-normalized REE patterns of the Dongchuan lavas. Chondrite values from Taylor and McLennan (1985).

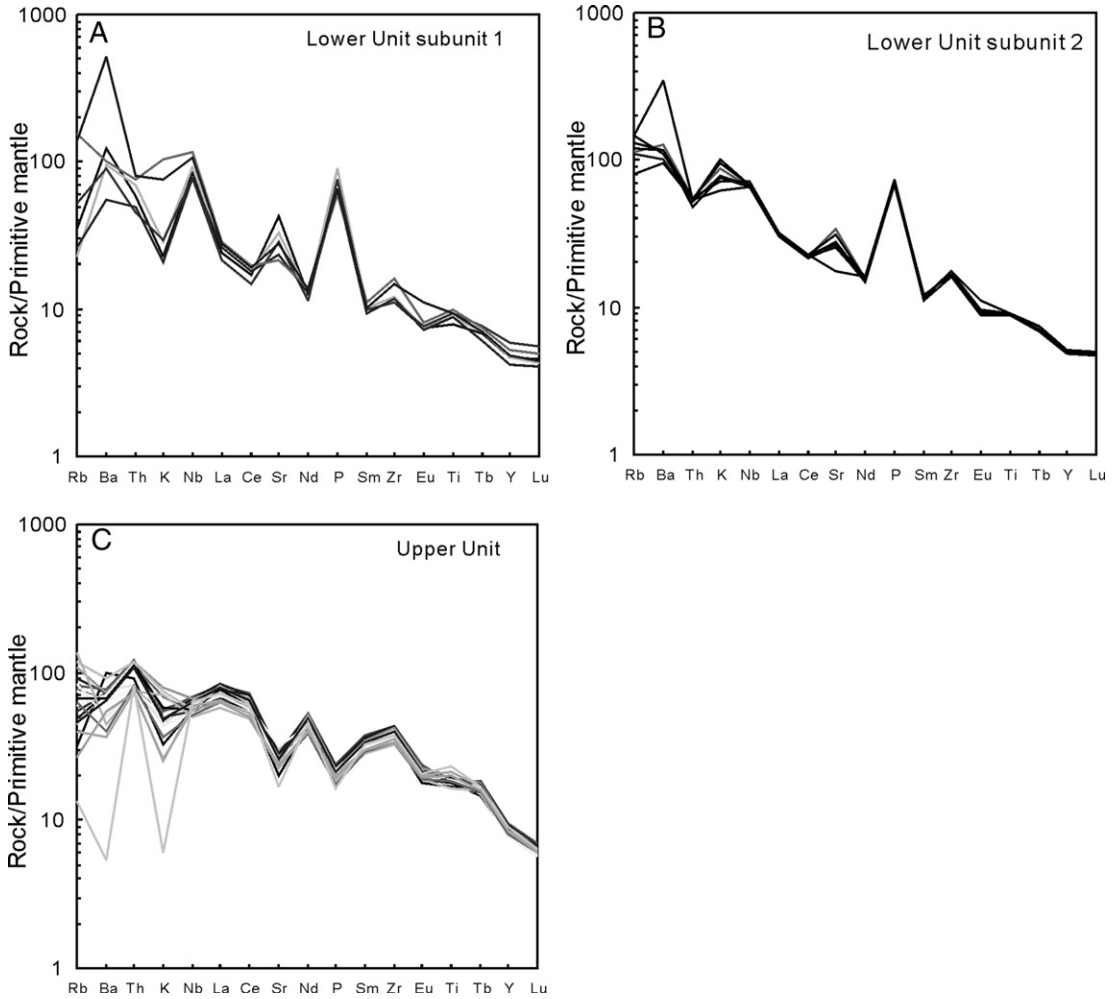

Fig. 7. Primitive mantle-normalized diagrams of incompatible elements for the Dongchuan lavas. Primitive mantle values from Hofmann (1988).

essentially constant as MgO decreases from 11.5 to 5.5 wt. %, whereas in the upper lavas it decreases from approximately 5.0 to 3.5 wt.% as MgO decreases (Fig. 5A). In both groups of lavas, P_2O_5 increases very slightly as MgO decreases, but samples from the two units plot in distinct fields (Fig. 25B). In general, lavas from both units show positive correlations between CaO and MgO although a few of the upper lavas are relatively depleted in CaO (Fig. 5C). Alumina correlates negatively with MgO in the Lower Unit lavas, but positively in the Upper Unit (Fig. 5D), whereas K_2O correlate negatively with MgO in the lavas of both units (Fig. 5E). The Lower Unit tephrites have relatively low Ni and Cr compared with the Upper Unit lavas at similar MgO contents, but both groups have similar trends (Fig. 5F and G). Rubidium generally increases with decreasing MgO in all the lavas, but it shows considerable scatter, suggesting minor alteration.

4.3. Incompatible elements

The lavas of the two units also have distinctive incompatible element compositions. Lower Unit lavas are marked by relatively low REE concentrations, e.g. 15.2–22.9 ppm La, 4.18–5.33 ppm Sm, and 2.02–2.89 ppm Yb, compared with 41.3–58.3 ppm La, 12.6–16.4 ppm Sm, and 3.08–3.82 ppm Yb in the Upper Unit basalts (Table 1). On chondrite-normalized REE diagrams, all of the lavas from both units exhibit steeply sloping patterns with distinct light rare-earth element (LREE) enrichment and those from the Upper Unit show the greatest enrichment (Fig. 6A, B and C). The Upper Unit basalts have REE contents and chondrite-normalized patterns similar to those of high-Ti basalts elsewhere in the ELIP (Xu et al., 2001; Song et al., 2001; Xiao et al., 2003; Zhou et al., 2006).

A striking geochemical feature of the Lower Unit tephrites is their significantly low abundances of HFSE except for Nb and Ta (e.g., 19.1–26.9 ppm Y, 123–195 ppm Zr, 3.19–4.77 ppm Hf, and 3.78–6.44 ppm Th), and high concentrations of low field strength elements (LFSE) (e.g., 370–899 ppm Sr and 382–3653 ppm Ba (Table 1). The Lower Unit lavas have low Zr/Nb ratios, ranging from 2.1 to 4.2, but high Ta/La ratios of 0.12 to 0.21 and Nb/Ta ratios of 16 to 19 (Table 1 and Fig. 4), In contrast, the Upper Unit lavas have high Zr/Nb ratios (9.3–10.1) and low Ta/La ratios (0.05 to 0.07) (Table 1, Fig. 4). Based on these ratios, the Lower Unit can be divided into two subunits; one with low Zr/Nb ratios (2.1–2.3) and high Nb/Y and Ta/La ratios (3.0–3.5 and 0.16–0.21, respectively), and the other with higher Zr/Nb ratios (3.7–4.2), and lower Nb/Y and Ta/La ratios (2.1–2.2 and 0.12–0.14, respectively (Table 1, Fig. 4).

In primitive mantle-normalized incompatible element diagrams, the Lower Unit tephrites display strongly positive Nb, Sr, and P anomalies and moderately positive Zr anomalies (Fig. 7A and B). In addition, the samples from subunit 1 of the Lower Unit have obviously negative K anomalies (Fig. 7A), whereas, those from subunit 2 display weak positive K anomalies and negative Th anomalies (Fig. 7B). In contrast, the Upper Unit lavas have relatively uniform primitive mantle-normalized incompatible element patterns and are characterized by negative P and Sr anomalies and weak positive Zr anomalies (Fig. 7C). Again, these characteristics are comparable with those of high-Ti basalts elsewhere in the ELIP (Song et al., 2001, 2004; Xiao et al., 2004).

4.4. Sr and Nd isotopes

The Lower Unit tephrites have initial $^{87}Sr/^{86}Sr$ values varying from 0.70689 to 0.70882 (Table 2), much higher than those of E-MORB and Hawaiian ocean island basalts (OIB) (Stille et al. 1983; Saunders et al., 1988). These values are also slightly higher than that of enriched mantle 1 (EM1), but much lower than those of enriched mantle 2 (EM2) and modern pelagic sediments (Stille et al., 1983; Saunders et al., 1988; Hoernle et al., 1991) (Fig. 8). All but one of the tephrites have $\varepsilon_{Nd\ (260\ Ma)}$ values ranging from −10.5 to −11.2, lower than EM1 and much lower than E-MORB and Hawaiian OIB. In contrast, the Upper Unit lavas have Sr and Nd isotopic values (Table 2) comparable with those of the ECFB elsewhere in the ELIP (Xu et al., 2001; Song et al., 2004; Zhong et al., 2004; Zhou et al., 2005) (Fig. 8).

5. Discussion

5.1. Fractional crystallization and crustal contamination

The presence of augite, amphibole, nepheline and olivine (with forsterite contents of 78–82) phenocrysts

Table 2
Rb–Sr and Sm–Nd isotopic ratios and abundances for the Dongchuan ECFB

	Rb (ppm)	Sr (ppm)	($^{87}Sr/^{86}Sr$) measured	($^{87}Sr/^{86}Sr$) (260 Ma)	Sm (ppm)	Nd (ppm)	($^{143}Nd/^{144}Nd$) measured	$\varepsilon_{Nd\ (260\ Ma)}$	$T_{(DM)}$ Ga
Lower Unit (Tephrite)									
YR04-3	87.1	584	0.708553±10	0.70696	4.58	18.3	0.511992±11	−11.10	2.40
YR04-5	32.7	600	0.707475±11	0.70689	4.42	15.5	0.512271±10	−6.38	2.60
YR04-6	16.9	497	0.708081±13	0.70772	4.18	17.6	0.511996±11	−10.78	2.18
YR04-7	71.3	714	0.709884±11	0.70882	5.07	21.2	0.511982±11	−11.08	2.22
YR04-9	93.7	562	0.710267±12	0.70848	5.19	21.8	0.512003±11	−10.62	2.15
YR04-11	82.3	657	0.709878±11	0.70854	5.12	21.5	0.511979±12	−11.13	2.21
YR04-13	50.9	541	0.709500±13	0.70849	4.86	20.5	0.511990±9	−10.87	2.17
Upper Unit (alkaline and tholeiitic basalt)									
YR04-15	48.8	418	0.707752±12	0.70650	13.0	58.6	0.512494±11	−0.72	1.07
YR04-17	47.9	619	0.706768±12	0.70594	13.5	59.8	0.512566±10	0.60	0.98
YR04-19	57.9	564	0.706941±11	0.70584	15.8	70.3	0.512586±12	0.99	0.94
YR04-21	30.4	587	0.706777±13	0.70622	16.1	71.1	0.512580±12	0.85	0.96
YR04-23	37.2	497	0.707698±13	0.70690	13.2	58.8	0.512485±10	−0.94	1.11
YR04-25	46.8	670	0.706998±12	0.70625	13.5	59.2	0.512571±11	0.65	0.98
YR04-27	75.3	557	0.708159±11	0.70671	13.2	59.4	0.512490±12	−0.82	1.08
YR04-29	29.3	540	0.706727±13	0.70615	14.8	65.6	0.512582±10	0.90	0.95
YR04-31	16.7	502	0.706168±11	0.70581	13.3	54.2	0.512637±11	1.60	0.98
YR04-33	8.6	358	0.706608±11	0.70635	14.5	63.2	0.512643±11	2.03	0.86

The values used in the T_{DM} calculations, such as $(^{143}Nd/^{144}Nd)_{DM,today}=0.513114$ and $(^{147}Sm/^{144}Nd)_{DM,\ today}=0.222$, are after Michard et al. (1985). The value of λ ($=6.54\times10^{-12}$) is after Lugmair and Marti (1978).

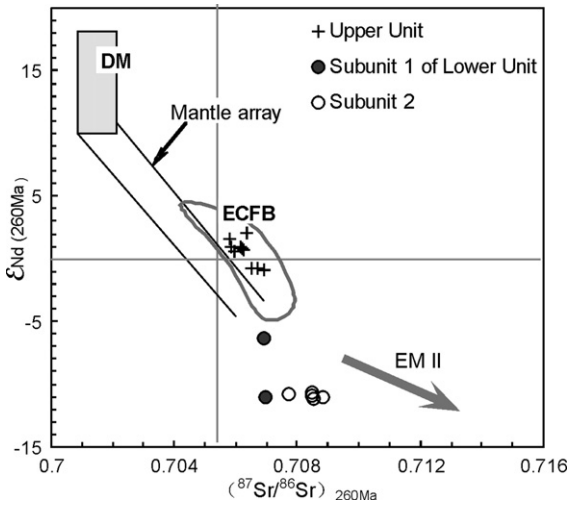

Fig. 8. Correlation of Nd–Sr isotopes for the Dongchuan lavas. The field of the ECFB is after Xu et al. (2001) and Xiao et al. (2004). DM, depleted mantle; EM I and EM II, enriched mantle, after Zindler and Hart (1986).

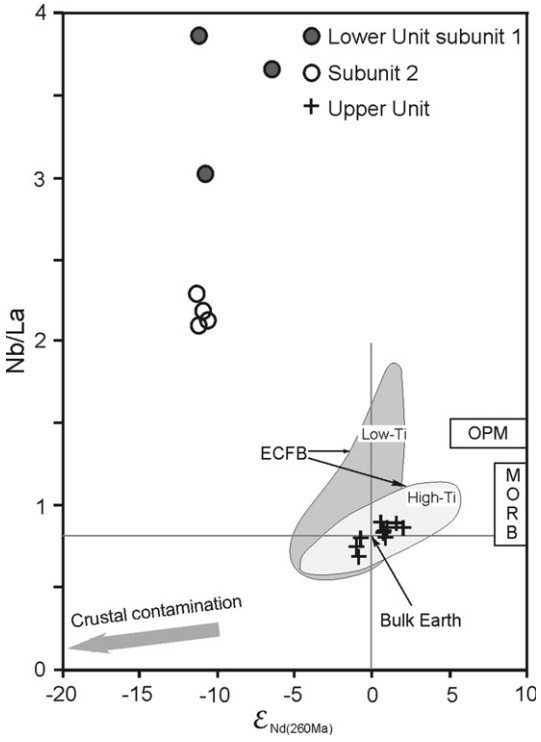

Fig. 10. Correlation between Nb/La and $\varepsilon_{Nd\ (260\ Ma)}$ for the Dongchuan lavas. The data for the ECFB are from Xu et al. (2001). OPM means average oceanic plume magma (Gibson et al. 1996).

in the Lower Unit tephrites indicates derivation from an alkaline parental magma that underwent extensive fractional crystallization of mafic minerals before eruption. The progressive increase in Al_2O_3 with decreasing MgO indicates an absence of significant plagioclase fractionation (Fig. 5), however, decreases in compatible elements, such as Cr and Ni, with decreasing MgO (Fig. 5) indicate extensive fractionation of pyroxene and olivine. In contrast, plagioclase phenocrysts in the Upper Unit lavas indicate significant crystallization of plagioclase. Although there are no olivine phenocrysts in the Upper Unit rocks, decreasing Al_2O_3, TiO_2, Cr, and Ni with decreasing of MgO suggests fractionation of olivine+clinopyroxene+plagioclase+Fe–Ti oxides (Fig. 5). Weak negative Eu anomalies also indicate fractionation of plagioclase in the Upper Unit basalts (Fig. 6).

Variable degrees of crustal assimilation are commonly expected for mantle-derived magmas migrating through continental crust to the surface (Hawkesworth et al., 1984; Mahoney, 1988; Carlson, 1991; Hergt et al., 1991). Nd and Sr isotope compositions and ratios between HFSE in

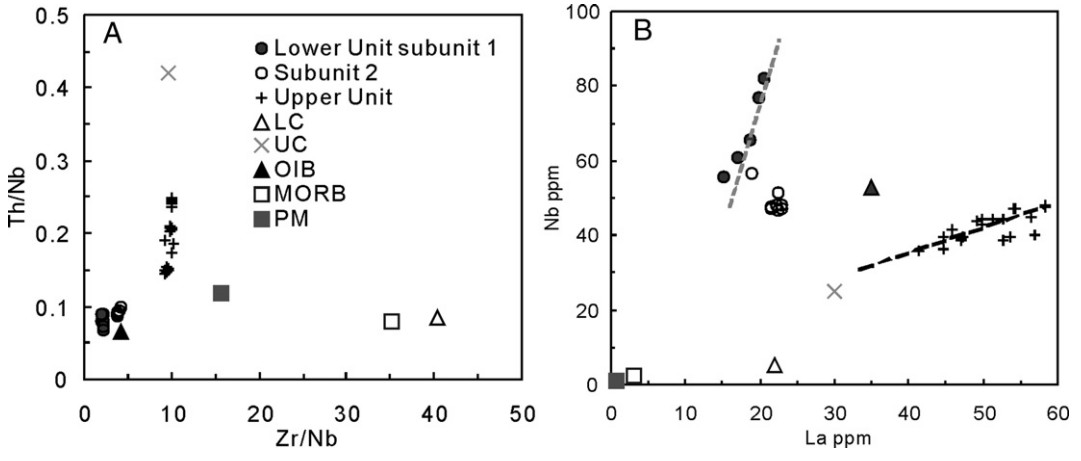

Fig. 9. Diagrams of Th/Nb versus La/Nb (A) and Nb versus La (B) for the Dongchuan lavas.

mafic rocks may be indicative of crustal contamination in an open magma system. The negative $\varepsilon_{Nd\ (260\ Ma)}$ values of the Lower Unit tephrites ranging from −10.5 to −11.2 and their relatively high $(^{87}Sr/^{86}Sr)_{260\ Ma}$ ratios varying from 0.70689 to 0.70882 (Table 2) could reflect significant crustal contamination. Some contamination is supported by a positive correlation between the $(^{87}Sr/^{86}Sr)_{260\ Ma}$ ratios of the tephrites and their SiO_2 contents and Zr/Nb ratios (Table 1). However, the trace element compositions provide strong evidence that the geochemistry of the tephrites was controlled primarily by their mantle source, rather than by crustal contamination. For example, the very low Th/Nb and Zr/Nb ratios (0.07–0.1 and 2.1–4.2, respectively) of the tephrites compared to crustal rocks (0.42–0.084 and 9.4–40, respectively) are not compatible with extensive crustal contamination. Instead, the Th/Nb and Zr/Nb ratios of the tephrites are similar to those of OIB (0.06 and 4.2, respectively) (Sun, 1980) (Fig. 9A). The very high Ta/La ratios (0.12–0.21) (Fig. 4) of the Lower Unit lavas also indicate little, if any, crustal contamination.

In addition, very extensive crustal contamination would be required to produce the negative $\varepsilon_{Nd\ (260\ Ma)}$ values of the tephrites (−10.5 to −11.2, mostly), and such contamination would also produce strong negative Nb anomalies in the primitive normalized trace element patterns. However, all the tephrites have very strong positive Nb anomalies relative to Th and La as shown in Fig. 7.

Thus, we conclude that, although some crustal contamination occurred, it was not an important factor controlling the compositions of the tephrites. Instead, the trace element and isotopic geochemistry of the tephrites reflect the chemical characteristics of their mantle source.

5.2. Two distinct mantle sources of the Dongchuan lavas

The most important chemical characteristics of the Lower Unit tephrites for determining their origin are: (1) low MgO (mostly 5.7–7.5 wt.%) and low compatible element concentrations, such as Ni and Cr (mostly less than 30 ppm and 42 ppm, respectively, (2) extremely low $\varepsilon_{Nd\ (260\ Ma)}$ (as low as −11) and high $^{87}Sr/^{86}Sr$ ratios (0.7070–0.7088), (3) highly positive Nb, Sr, and P anomalies in the primitive mantle-normalized incompatible element diagrams (Fig. 7A and B), and (4) low incompatible element concentrations and LREE-enriched chondrite-normalized REE patterns (Fig. 5A and B).

The low concentrations of MgO, Ni, Cr and REE, coupled with high alkali contents in these rocks could reflect low degrees of partial melting of a depleted source

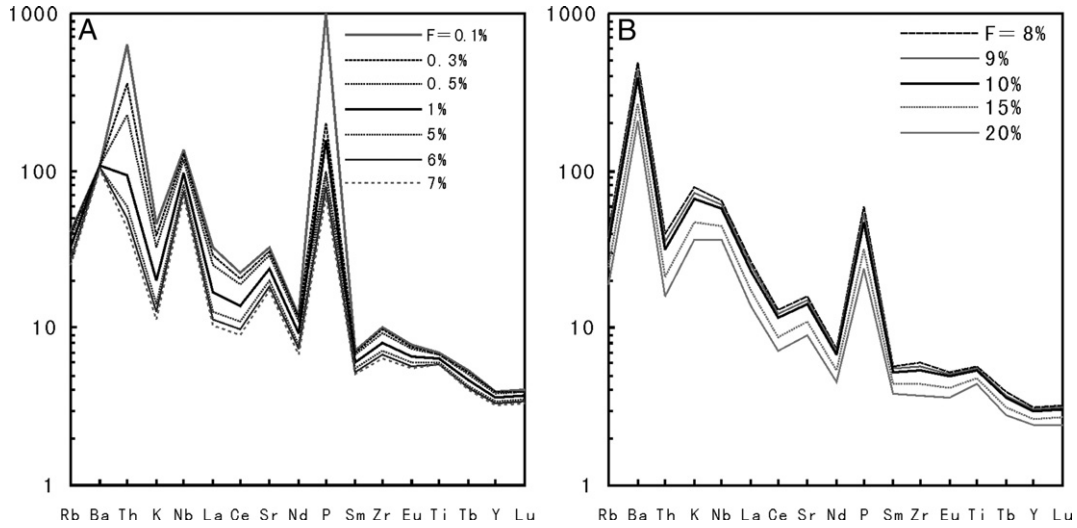

Fig. 11. Primitive mantle-normalized incompatible element patterns for the magmas generated by batch melting of volatile-mineral bearing spinel lherzolite under degrees of partial melting (F) of less than 0.7% (A) and more than 8% (B). K an P were treated as stoichiometric constituents of phlogopite and apatite, respectively. Source mineralogy: 57% olivine, 25% orthopyroxene, 9% clinopyroxene, 5% spinel, 4% amphibole, 2% phlogopite, and 0.2% apatite, melting in proportions of 0.3, 0.25, 0.35, 0.05, 0.04, 0.007, and 0.003, respectively after the volatile minerals were exhausted (F=7%), olivine, orthopyroxene, clinopyroxene, and spinel are assumed to melt in proportions of 0.3, 0.25, 0.44, 0.01, respectively. Concentrations of incompatible elements of the volatile mineral-bearing spinel lherzolite were calculated using a mode of spinel lherzolite (93.8%), amphibole (4%), phlogopite (2%), and apatite (0.2%). We assumed that the trace element concentrations of the spinel lherzolite were the same as those of the primitive mantle. The incompatible element data are from McDonough et al. (1992), and Ionov et al. (1997) (Table 3). Mineral/basaltic melt partition coefficients are from Arth (1976), Fujimaki et al. (1984), and Ionov et al. (1997) (Table 4).

Table 3
Concentrations of incompatible elements in primitive mantle and volatile minerals in lithosphere xenoliths

	Primitive mantle	Hb in vein	Ph in vein	Ap in vein
Rb	0.635	1.34	98	0.105
Ba	6.99	32.1	14610	118
Th	0.084	0.024	0.008	95.2
K	240	6640	69460	0
Nb	0.713	143	7.08	2.66
La	0.708	1.75	0	765
Ce	1.833	5.38	0.15	623
Sr	21.1	191	662	4087
Nd	1.366	5.52	0.053	87
P	92	0	0	174648
Sm	0.444	2.04	0.012	13.9
Zr	11.2	28.7	3.59	0.87
Eu	0.168			
Ti	1280	13430	28240	0
Tb	0.108			
Y	4.55			
Lu	0.0737			

Data of the primitive mantle from McDonough et al. (1992), data of amphibole (Hb), phlogopite (Ph), and apatite (Ap) from Ionov et al. (1997).

followed by fractional crystallization. However, there are several reasons to question derivation from a depleted source. First, the relative enrichment of Nb and Ta compared with REE and other incompatible elements must be a feature of the source because these elements are not obviously fractionated from each other during partial melting and fractional crystallization. Secondly, the high P_2O_5 contents of the tephrites (>1.0 wt.%) are difficult to explain by fractional crystallization of a magma derived from a depleted source. Finally, the $\varepsilon_{Nd\ (260\ Ma)}$ values of the tephrites are too low be derived from depleted mantle (Zindler and Hart, 1986), and their Nb/La ratios are much higher than the rest of the ECFB (Song et al., 2004; Xu et al., 2001; Xiao et al., 2004) (Fig. 10).

An early study by Chung and Jahn (1995) suggested that the ECFB were formed by plume-derived melts mixed with small amounts of lamproitic melt generated in the lithospheric mantle. However, no lamprophyres have thus far been found in the Emeishan LIP and later workers argued that the geochemistry of the ECFB was produced by interaction of the plume melts with a lithospheric mantle previously contaminated by subducted material (Song et al. 2001, 2004; Xiao et al. 2004). The tephrites described in the current study provide the first unambiguous evidence for melting of the base of the metamorphosed lithospheric mantle beneath the Emeishan LIP.

Hornblende phenocrysts in the Lower Unit tephrites provide evidence of low but significant H_2O contents in the parental magma. The absence of plagioclase phenocrysts in the tephrites and the regular increase of Al_2O_3 with decreasing MgO also indicate a hydrous melt in which clinopyroxene crystallized earlier than plagioclase (Yoder 1976). The high positive Nb, Sr, and P anomalies in the primitive mantle-normalized incompatible element patterns, extremely high Ta/La ratios and extremely negative $\varepsilon_{Nd\ (260\ Ma)}$ values for these rocks (Table 1), coupled with evidence of only weak crustal contamination, suggest that the primary magmas of the tephrites were generated from a metasomatized mantle source containing volatile-bearing minerals. The positive Sr and P anomalies could possibly reflect fractionation of plagioclase and apatite, but the absence of such minerals in the tephrites suggests that these anomalies are a feature of the mantle source.

According to phlogopite/silicate melt partition coefficients, Ba, Rb, and Ti can be strongly concentrated in phlogopite, whereas REE, Th, and Zr are strongly incompatible for this mineral (Ionov et al. 1997). Both LFSE and HFSE are moderately incompatible for amphibole, therefore concentrations of these elements in amphibole are much higher than in anhydrous minerals, such as olivine and pyroxene, in the metasomatized mantle. Phosphorus, REE, Ba, Th and Sr are strongly concentrated in apatite because of their high apatite/melt partition coefficients (Ionov et al. 1997). Thus, the significant positive Nb, P, and Sr anomalies and positive and negative K anomalies of the tephrites (Fig. 7) indicate that apatite, amphibole and phlogopite were present in the mantle

Table 4
Mineral/basaltic melt partition coefficients

	Ol	Opx	Cpx	Sp	Hb	Ph	Ap
Rb	0.0098	0.022	0.031	–	0.53	8.2	0.01
Ba	0.0099	0.026	0.0006	–	0.54	48	0.74
Th	–	–	0.0056	–	0.0056	0.0005	0.65
K	0.0068	0.014	0.038	–	–	–	–
Nb	0.01	0.15	0.0027	0.4	0.14	0.081	0.001
La	0.007	0.02	0.044	0.1	0.061	0.028	4
Ce	0.006	0.02	0.084	0.07	0.114	0.0006	4.2
Sr	0.014	0.04	0.096	0	0.32	0.15	2.7
Nd	0.006	0.03	0.173	0.06	0.22	0.0006	3.4
Sm	0.007	0.05	0.28	0.05	0.33	0.0008	3.1
Zr	0.012	0.18	0.12	0.1	0.18	0.026	0.007
Eu	0.007	0.05	0.31	0.03	0.36	–	2.8
Ti	0.02	0.1	0.4	0.2	1.5	2.5	–
Tb	0.009	0.1	0.36	0.01	0.37	0.0027	2.2
Y	0.01	0.18	0.44	0.1	0.53	0.018	3.1
Lu	0.045	0.42	0.27	0.015	0.41	0.028	0.75

The partition coefficients are from Arth (1976), Fujimaki et al. (1984), and Ionov et al. (1997).

source. Amphibole is thermally unstable in both the convecting asthenospheric upper mantle and in thermal mantle plumes, but stable in old SCLM (Class and Goldstein 1997). Thus, the presence of amphibole in the metasomatised mantle source of the Lower Unit tephrites indicates that the source was most likely within the SCLM. The occurrence of tephrites only in the Dongchuan area implies that metasomatism in the SCLM was not extensive beneath the Yangtze craton. In the Parana LIP, compositional heterogeneity in the upper mantle occurs over a few hundred km (Peate and Hawkesworth, 1996), whereas xenoliths from a restricted area within South Africa indicate that considerable local heterogeneity can occur over a vertical distance of 50 km in the lithospheric mantle (Water and Erlank, 1988).

Fig. 11 illustrates that the positive Nb, Sr, and P anomalies and negative K anomalies in the primitive mantle-normalized incompatible element patterns of the Lower Unit tephrites can be generated by melting of a volatile mineral-bearing mantle source. It is assumed that the metasomatised mantle source is spinel lherzolite containing amphibole, phlogopite, and apatite. Proportions of melt minerals are assumed to be 0.3 olivine, 0.25 orthopyroxene, 0.35 clinopyroxene, 0.05 spinel, 0.04 amphibole, 0.007 phlogopite, and 0.003 apatite.

According to modeling calculations used in this study, magmas generated by less than 7% partial melting would have low K contents because phlogopite (contains ~9 wt.% K_2O) would not be completely melted (Ionov et al., 1997). With such low degrees of partial melting, amphibole may also be a residual phase, which could account for the low Zr concentrations in the lavas of subunit 1 of the Lower Unit. Zirconium is concentrated in amphibole in lithospheric xenoliths and has a mineral/melt partition coefficient for amphibole larger than those for phlogopite and apatite (Ionov et al., 1997). The release of Nb, Sr, and Ba from amphibole, phlogopite and apatite during partial melting would cause positive anomalies for Sr and Ba. With the increasing degrees of partial melting, the concentrations of the incompatible elements would be diluted, particularly Th and P, which are incompatible in these volatile-bearing minerals and highly concentrated in apatite in lithospheric xenoliths (Ionov et al., 1997). Under extremely low degrees of partial melting, e.g. less than 0.1%, the magma would have extremely high positive P anomalies and variable positive Th anomalies as shown in the Fig. 11A. The primitive mantle-normalized incompatible element patterns of the magmas generated by 0.5–0.7% partial melting of such a metasomatised spinel lherzolite are consistent with those of the subunit 1 tephrites of the Lower Unit (Figs. 7A and 11A).

Once amphibole has been consumed, further melting will cause a decrease in the Nb content. As shown in Fig. 9B, the lavas of subunit 1 have highly variable Nb contents, suggesting various degrees of partial melting.

Larger degrees of partial melting (>8%) of such a metasomatised mantle source would produce primitive magmas having positive anomalies not only for Sr and P, but also for K, because these elements would be released from the volatile-bearing minerals (Fig. 11B). The primitive mantle-normalized incompatible element patterns of the magmas produced by such high degrees of partial melting compare well with those of the subunit 2 tephrite of the Lower Unit (Figs. 7B and 11B). Thus, we propose that the primary magmas of the subunit 1 and 2 tephrites were formed by different degrees of partial melting of the volatile mineral-bearing metasomatized spinel lherzolite in the SCLM; <5–8% for subunit 1 and >8%) for subunit 2.

In contrast, the Upper Unit lavas are characterized by: (1) an absence of volatile-bearing phenocrysts, (2) steeply right-inclined chondrite-normalized REE patterns with Ta/La ratios slightly higher than those of the primitive mantle and (3) Sr and Nd isotopic ratios comparable to typical high-Ti basalts elsewhere in the ELIP (Xu et al., 2001; Song et al., 2004; Xiao et al., 2004).

The absence of volatile-bearing minerals and the presence of plagioclase phenocrysts in the Upper Unit lavas suggest that the parental magmas were dry, and the Ta/La ratios similar to the primitive mantle indicate little or no crustal contamination. These distinctive chemical characteristics indicate that the Upper Unit lavas were derived from the same source as the high-Ti basalts elsewhere in the ELIP (Song et al., 2001, 2004; Xu et al., 2001; Xiao et al., 2004). Detailed geochemical studies of the ELIP indicate that the high-Ti lavas were derived from a mantle plume and then contaminated by subducted materials in the SCLM before being erupted (Song et al., 2001; Xiao et al., 2004).

5.3. Petrogenetic implications

Theoretical considerations (McKenzie, 1989) and the analysis of micro-inclusions in diamonds (Navon et al., 1988) indicate the presence of small volume melt fractions rich in potassium, incompatible elements, water, and carbonate in the asthenosphere. Such melts are concentrated at base of the lithosphere and form enriched domains resulting in chemical heterogeneity in the lithospheric mantle (Menzies, 1990; Saunders et al., 1991, 1992; Hawkesworth et al., 1993; Ionov and

Hofmann, 1995). Studies of mantle xenoliths in alkaline basalts indicate that volatile-bearing minerals, such as amphibole, phlogopite and apatite, in the metasomatised mantle are generally enriched in LFSE, Nb, Ta, K and P (Mertes and Schmincke, 1985; Wilson and Downes, 1991; Hoernle and Schmincke, 1993; Class et al., 1994; Ionov and Hofmann, 1995; Ionov et al., 1997). The Archaean lithospheric mantle has wide ranges of ε_{Nd} (>+10 to <−30), whereas the values of ε_{Nd} of the Proterozoic and Phanerozoic lithospheric mantle are rarely lower than −10 (Menzies, 1990). The low ε_{Nd} of the Archaean lithospheric mantle may have been achieved by migration of small volume partial melts and/or fluids from the asthenospheric mantle (Menzies, 1990). The metasomatised domains may then be melted because of thermal perturbations associated with a plume to generate alkaline basaltic magmas (McKenzie, 1989). Many flood basalt provinces, such as the Karoo, Parana, and Siberia, contain at least some volcanic units produced by 'wet' melting of SCLM containing hydrous minerals, or by mixing of plume-derived picritic melts with ultrapotassic melts as they rose through the lithospheric mantle (Ellam and Cox, 1991; Lightfoot et al., 1990, 1993; Gallagher and Hawkesworth, 1992; Gibson et al., 1996; Jackson and Rigden, 1998; Zhang and O'Reilly, 1997).

Depleted mantle model ages (T_{DM}) of the Lower Unit tephrites, ranging from 2.15 to 2.60 Ga (Table 2), suggest a very old, perhaps Archean, SCLM in the Dongchuan region. The high Nb/La ratios (up to 3.9), low K_2O contents (<3 wt.%), and especially the very low REE of the tephrites rule out a relationship to lamproites, which have low Nb/La ratios, very high K_2O, and high incompatible elements (Mitchell and Bergman, 1991). Thus, the mantle source of the Lower Unit tephrites is most likely very old SCLM modified by volatile-rich melts or fluids from the asthenosphere.

White and McKenzie (1995) proposed that small amounts of magma could be formed at the base of the lithospheric mantle due to heating by mantle plumes during the initial stages of continental flood basalt activity. Experimental studies indicate that the solidus temperature of wet peridotite, containing small amounts of H_2O (0.3–0.4 wt.%) and CO_2, is about 250° K lower than that of dry peridotite at mantle depths of 40–70 km (Wyllie, 1981; Wallace and Green, 1988). It is possible that thinning of the lithosphere caused by upwelling of the Emeishan mantle plume (He et al., 2003) may have led to decompressional melting of the metasomatized SCLM. In contrast, the geochemical similarities between the Upper Unit basalts at Dongchuan and the high-Ti ECFB elsewhere suggest that these rocks were derived from magmas produced by decompression melting of the plume head (Song et al., 2001; Xu et al., 2001; Zhou et al., 2006).

The chemostratigraphic variations of the Dongchuan lavas provide valuable data on the nature of generation of basaltic magmas and plume-SCLM interaction during mantle plume upwelling. When the mantle plume ascended to the base of the SCLM, the SCLM was thinned and alkaline basaltic melts were produced by partial melting of the volatile mineral-bearing domains due to heating bt the plume and to decompression. The alkaline basaltic melts formed in only a few areas because of the heterogeneous nature of the SCLM. Finally, decompressional melting of the mantle plume produced great quantities of basaltic magma with OIB-like geochemical features, which were then erupted to form the dominant Emeishan flood basalts.

6. Conclusions

Alkaline tephrites, cropping out at the base of the Emeishan flood basalts in the Dongchuan area, are characterized by highly negative $\varepsilon_{Nd\ (t)}$ and positive Nb, Sr, and P anomalies in primitive mantle-normalized incompatible element diagrams. Their chemical and isotopic compositions distinguish them from the high-Ti basalts that make up the bulk of the lavas in the ELIP. The tephrites were derived by partial melting of a metasomatised domain at the base of the SCLM in the spinel stability field, triggered by the rising Emeishan plume. In contrast, the overlying high-Ti basalts were generated by decompressional melting of the Emeishan mantle plume in the garnet stability field.

Acknowledgments

This study was funded by the National Natural Science Foundation of China (NSFC 40373030 and 4057314) and "CAS Hundred Talents" Project from Chinese Academy of Sciences to Song X.-Y. Dr. Lu J.-J. from the Department of Earth Sciences, Nanjing University is thanked for his help with the chemical analyses of trace elements. We also thank Dr. Feng C.-X. for her help on oxide analyses by XRF in our Institute as well as Martin Menzies and Akira Ishawatari for their insightful and constructive comments on our manuscript.

References

Ali, J.R., Thompson, G.M., Song, X.-Y., 2002. Emeishan Basalts (SW China) and the 'end-Guadalupian' crisis: magnetobiostratigraphic constraints. Journal of the Geological Society, London 159, 21–29.

Ali, J.R., Thompson, G.M., Zhou, M.-F., Song, X.-Y., 2005. Emeishan large igneous province, SW China. Lithos 79, 475–489.

Arndt, N.T., Chauvel, C., Czamanske, G., Fedorenko, V., 1998. Two mantle sources, two plumbing systems: tholeiitic and alkaline magmatism of the Meymecha River Basin, Siberian flood volcanic province. Contributions to Mineralogy and Petrology 133, 297–313.

Arndt, N.T., Christensen, U., 1992. The role of lithospheric mantle in continental flood volcanism: thermal and geochemical constraints. Journal of Geophysical Research 97, 10967–10981.

Arth, J.G., 1976. Behavior of trace elements during magmatic processes — a summary of the theoretical models and their applications. U. S. Geological Survey Journal of Research 4, 43–47.

Carlson, R.W., 1991. Physical and chemical evidence on the cause and source characteristics of flood basalt volcanism. Australian Journal of Earth Sciences 38, 525–544.

Chung, S.L., Jahn, B.M., 1995. Plume–lithosphere interaction in generation of the Emeishan flood basalts at the Permian–Triassic boundary. Geology 23, 889–892.

Class, C., Altherr, R., Volker, F., Eberz, G., McCulloch, M.T., 1994. Geochemistry of Pliocene to Quaternary alkali basalts from the Huri Hills, northern Kenya. Chemical Geology 113, 1–22.

Class, C., Goldstein, S.L., 1997. Plume–lithosphere interactions in the ocean basins: constraints from the source mineralogy. Earth and Planetary Science Letters 150, 245–260.

Ellam, R.M., Cox, K.G., 1991. An interpretation of Karoo picritic basalts in terms of interaction between asthenospheric magmas and mantle lithosphere. Earth and Planetary Science Letters 105, 330–342.

Fujimaki, H., Tatsumoto, M., Aoki, K., 1984. Partition coefficients of Hf, Zr and REE between phenocrysts and groundmasses. Proceedings of the Fourteenth Lunar and Planetary Science Conference, Part 2, Journal of Geophysical Research 89, B662–B672.

Gallagher, K., Hawkesworth, C., 1992. Dehydration melting and the generation of continental flood basalts. Nature 358, 57–59.

Gibson, S.A., Thompson, R.N., Dikin, A.P., Leonardos, O.H., 1996. Erratum to "High-Ti and low-Ti mafic potassic magmas: key to plume–lithosphere interactions and continental flood-basalt genesis". Earth and Planetary Science Letters 141, 325–341.

GMBS (Geology and Mineral Resource Bureau of Sichuan Province), 1991. The Regional Geology of Xizhang. Geological Publishing House, Beijing. (in Chinese).

GMBY (Geology and Mineral Resource Bureau of Yunnan Province), 1978. 1/200000 geological survey report of the Dongchuan region. (in Chinese).

Hawkesworth, C.J., Rogers, N.W., Vancalsteren, P.W.C., 1984. Mantle enrichment processes. Nature 311, 331–335.

Hawkesworth, C.J., Gallagher, K., Hergt, J.M., McDermott, F., 1993. Trace element fractionation processes in the generation of island arc basalts. Philosophical Transactions of the Royal Society London A 342, 179–191.

He, B., Xu, Y.-G., Chung, S.-L., Xiao, L., Wang, Y.-M., 2003. Sedimentary evidence for a rapid, kilometer-scale crustal doming prior to the eruption of the Emeishan flood basalts. Earth and Planetary Science Letters 213, 391–405.

Hergt, J.M., Peate, D.W., Hawkesworth, C.J., 1991. The petrogenesis of Mesozoic Gondwana low-Ti flood basalts. Earth and Planetary Science Letters 105, 398–416.

Hoernle, K., Schmincke, H.-U., 1993. The petrology of the tholeiites through melilite nephelinites on Gran Canaria, Canary Islands: crystal fractionation, accumulation, and depths of melting. Journal of Petrology 34, 573–597.

Hoernle, K., Tilton, G., Schmincke, H.-U., 1991. Sr–Nd–Pb isotope evolution of Gran Canaria: evidence for shallow enriched mantle beneath the Canary Islands. Earth and Planetary Science Letters 106, 44–63.

Hofmann, A.W., 1988. Chemical differentiation of the Earth: the relationship between mantle, continental crust, and oceanic crust. Earth and Planetary Science Letters 90, 297–314.

Ionov, D.A., Hofmann, A.W., 1995. Nb–Ta-rich mantle amphiboles and micas: implication for subduction-related metasomatic trace element fractionation. Earth and Planetary Science Letters 131, 341–356.

Ionov, D.A., Griffin, W.L., O'Reilly, S.Y., 1997. Volatile-bearing minerals and lithophile trace elements in the upper mantle. Chemical Geology 141, 153–184.

Irvine, T.N., Baragar, W.R.A., 1971. A guide to the chemical classification of the common volcanic rocks. Canadian Journal of Earth Sciences 8, 523–548.

Jackson, I., Rigden, S.M., 1998. Composition and temperature of the earth's mantle: seismological models interpreted through experimental studies of earth materials. In: Jackson, I. (Ed.), The Earth's Mantle-Composition, Structure, and Evolution. The Press Syndicate of The Cambridge University, United Kingdom.

Le Maitre, R.W., Bateman, P., Dudek, A., Keller, J., Lameyre Le Bas, M.J., Sabine, P.A., Schmid, R., Sorensen, H., Streckeisen, A., Woolley, A.R., Zanettin, B., 1989. A Classification of Igneous Rocks and Glossary of Terms. Blackwell, Oxford.

Lightfoot, P.C., Naldrett, A.J., Gorbachev, N.S., Doherty, W., Fedorenko, V.A., 1990. Geochemistry of the Siberian Trap of the Noril'sk area, USSR, with implications for the relative contributions of crust and mantle to flood basalt magmatism. Contributions to Mineralogy and Petrology 104, 631–644.

Lightfoot, P.C., Hawkesworth, C.J., Hergt, J., Naldrett, A.J., Gorbachev, N.S., Fedorenko, V.A., 1993. Remobilisation of the continental lithosphere by a mantle plume: major-, trace-element and Sr-, Nd-, and Pb-isotope evidence from picritic and tholeiitic lavas of the Noril'sk District, Siberian Trap, Russia. Contributions to Mineralogy and Petrology 114, 171–188.

Lugmair, G.W., Marti, K., 1978. Lunar initial $^{143}Nd/^{144}Nd$: differential evolution of the lunar crust and mantle. Earth and Planetary Science Letters 39, 349–357.

Mahoney, J.J., 1988. Deccan Traps. In: Macdougall, J.D. (Ed.), Continental Flood Basalts. Kluwer Academic Publishers, Dordrecht.

McDonough, W.F., Sun, S., Ringwood, A.E., Jagoutz, E., Hofmann, A.W., 1992. K, Rb and Cs, in the earth and moon and the evolution of the earth's mantle. Geochimica et Cosmochimica Acta 56, 1001–1012.

McKenzie, D., 1989. Some remarks on the movement of small melt fractions in the mantle. Earth and Planetary Science Letters 95, 53–72.

McKenzie, D.P., Bickle, M.J., 1988. The volume and composition of melt generated by extension of the lithosphere. Journal of Petrology 29, 625–679.

Menzies, M.A., 1990. In: Menzies, M.A. (Ed.), Archaean, Proterozoic, and Phanerozoic Lithospheres. Oxford University Press, Continental Mantle.

Mertes, H., Schmincke, H.-U., 1985. Mafic potassic lavas of the Quaternary West Eifel volcanic field I. Major and trace elements. Contributions to Mineralogy and Petrology 89, 330–345.

Michard, A., Gurriet, P., Soudant, M., Albarede, F., 1985. Nd isotopes in French Phanerozoic shales: external vs internal aspects of crustal evolution. Geochimica et Cosmochima Acta 49, 601–610.

Mitchell, R.H., Bergman, S.C., 1991. Petrology of Lamproites. Plenum, New York.

Navon, O., Hutcheon, I.D., Rossman, G.R., Wasserburg, G.J., 1988. Mantle-derived fluids in diamond micro-inclusions. Nature 335, 784–789.

Peate, D.W., Hawkesworth, C.J., 1996. Lithospheric to asthenospheric transition in Low-TI flood basalts from southern Parana, Brazil. Chemical Geology 127, 1–24.

Saunders, A.D., Norry, M.J., Tarney, J., 1988. Origin of MORB and chemically depleted mantle reservoirs: trace element constraints. Journal of Petrology 415–445 Special Lithosphere Issue.

Saunders, A.D., Norry, M.J., Tarney, J., 1991. Fluid influence on the trace element composition of subduction zone magmas. Transactionss of the Royal Society London A 335, 377–392.

Saunders, A.D., Storey, M., Kent, R.W., Norry, M.J., 1992. Consequences of plume–lithosphere interactions. In: Storey, B.C., Alabaster, T., Pankhurst, R.J. (Eds.), Magmatism and the Causes of Continental Break-up. Geological Society London Special Publication, 68, pp. 41–60.

Song, X.-Y., Wang, Y.-L., Cao, Z.-M., Li, Y.-G., Wen, C.-Q., 1998. Emeishan basalts, Emei tafrogeny and mantle plume. Geology-Geochemistry 12 (1), 47–52 (in Chinese).

Song, X.-Y., Zhou, M.-F., Hou, Z.-Q., Cao, Z.-M., Wang, Y.-L., Li, Y.-G., 2001. Geochemical constraints on the mantle source of the Upper Permian Emeishan Continental Flood Basalts, Southwestern China. International Geology Review 43, 213–225.

Song, X.-Y., Zhou, M.-F., Cao, Z.-M., Robinson, P.T., 2004. Late Permian rifting of the South China Craton caused by the Emeishan mantle plume. Journal Geological Society London 161, 773–781.

Song, X.-Y., Zhong, H., Zhou, M.-F., Tao, Y., 2005a. Magmatic sulfide deposits in the Permian Emeishan Large Igneous Province, SW China. In: Mao, J.W., Bierlein, F.P. (Eds.), Mineral Deposit Research: Meeting the Global Challenge. Springer, Berlin.

Song, X.-Y., Zhang, C.-J., Hu, R.-Z., Zhong, H., Zhou, M.-F., Ma, R.-Z., Li, Y.-G., 2005b. Genetic links of magmatic deposits in the Emeishan large igneous province with dynamics of mantle plume. Kungwu Yanshi 25, 35–44 (in Chinese with English abstract).

Song, X.-Y., Zhou, M.-F., Keays, R.R., Cao, Z.-M., Sun, M., Qi, L., 2006. Geochemistry of the Emeishan flood basalts at Yangliuping, Sichuan, SW China: implications for sulfide segregation. Contributions to Mineralogy and Petrology 152, 53–74.

Stille, P., Unruh, D.M., Tatsumoto, M., 1983. Pb, Sr, Nd, and Hf isotopic evidence of multiple sources for Oahu, Hawaii basalts. Nature 304, 25–29.

Sun, S.S., 1980. Lead isotopic study of young volcanic rocks from mid-oceanic ridges, ocean islands and island arcs. Philosophical Transactions of the Royal Society A297, 409–445.

Taylor, S.R., McLennan, S.M., 1985. The Continental Crust: Its Composition and Evolution. Blackwell, Oxford.

Thompson, G.M., Ali, J.R., Song, X.-Y., 2001. Emeishan Basalts, southwest China: reappraisal of the formation's type area stratigraphy and a discussion of its significance as a LIP. Journal of the Geological Society, London 158, 593–599.

Turner, S., Hawkesworth, C., Gallagher, K., Stewart, K., Peate, D., Mantovani, M., 1996. Mantle plumes, flood basalts, and thermal models for melt generation beneath continents: assessment of a conductive heating model and application to the Parana. Journal of Geophysical Research 101, 11503–11518.

Wallace, M.E., Green, D.H., 1988. An experimental determination of primary carbonatite magma composition. Nature 335, 343–346.

Water, F., Erlank, A.J., 1988. Assessment of the vertical extent and distribution of mantle metasomatism below Kimberley, South Africa. In: Martin, M.A., Cox, K.G. (Eds.), Oceanic and Continental Lithosphere: Similarities and Differences. Oxford University Press.

White, R.S., McKenzie, D.P., 1989. Magmatism at rift zones: the generation of volcanic continental margins and flood basalts. Journal of Geophysical Research 94, 7685–7729.

White, R.S., McKenzie, D.P., 1995. Mantle plumes and flood basalts. Journal of Geophysical Research 100, 17543–17585.

Wilson, M., Downes, H., 1991. Tertiary–Quaternary extension-related alkaline magmatism in western and central Europe. Journal of Petrology 32, 811–849.

Wyllie, P.J., 1981. Plate tectonics and magma genesis. Geologische Rundschau 70, 128–153.

Xiao, L., Xu, Y.-G., Chung, S.L., He, B., Mei, H., 2003. Chemostratigraphic correlation of Upper Permian lava succession from Yunnan Province, China: Extent of the Emeishan igneous province. International Geology Review 45, 753–766.

Xiao, L., Xu, Y.G., Mei, H.J., Zheng, Y.F., He, B., Piranjno, F., 2004. Distinct mantle sources of low-Ti and high-Ti basalts from the western Emeishan large igneous province, SW China: implications for plume–lithosphere interaction. Earth and Planetary Science Letters 228, 525–546.

Xu, Y.-G., Chung, S.L., Jahn, B.M., Wu, G.-Y., 2001. Petrologic and geochemical constraints on the petrogenesis of Permian–Triassic Emeishan flood basalts in southwestern China. Lithos 58, 145–168.

Xu, Y.-G., He, B., Chung, S.-L., Menzies, M.A., Frey, F.A., 2004. Geologic, geochemical, and geophysical consequences of plume involvement in the Emeishan flood-basalt province. Geology 32, 917–920.

Yoder, H.S., 1976. Generation of Basaltic Magma. National Academy of Sciences, Washington DC.

Zhang, M., O'Reilly, S.Y., 1997. Multiple sources for basaltic rocks from Dubbo, eastern Australia: geochemical evidence for mantle-lithospheric plume interaction. Chemical Geology 136, 33–54.

Zhang, Y.-X., Luo, Y.-N., 1988. Panxi Rifting. Geological Publication House, Beijing. (in Chinese).

Zhang, M., Stephenson, P.J., O'Reilly, S.Y., McCulloch, M., Norman, M., 2001. Petrogenesis and geodynamic implications of Late Cenozoic basalts in north Queensland, Australia: trace-element and Sr–Nd–Pb isotope evidence. Journal of Petrology 42, 685–719.

Zhong, H., Yao, Y., Prevec, S.A., Wilson, A.H., Viljoen, M.J., Viljoen, R.P., Liu, B.-G., Luo, Y.-N., 2004. Trace-element and Sr–Nd isotopic geochemistry of the PGE-bearing Xinjie layered intrusion in SW China. Chemical Geology 203, 237–252.

Zhou, M.-F., Yan, D.-P., Kennedy, A.K., Li, Y., 2002a. SHRIMP U–Pb zircon geochronological and geochemical evidence for Neoproterozoic arc-magmatism along the western margin of the Yangtze Block, South China. Earth and Planetary Science Letters 196, 51–67.

Zhou, M.-F., Zhao, T.-P., Malpas, J., Sun, M., 2000. Crustal-contaminated komatiitic basalts in Southern China: products of a Proterozoic mantle plume beneath the Yangtze Block. Precambrian Research 103, 175–189.

Zhou, M.-F., Malpas, J., Song, X.-Y., Robinson, P.T., Sun, M., Kennedy, A.K., Lesher, C.M., Keays, R.R., 2002b. A temporal link between the Emeishan Large Igneous Province (SW China) and the end-Guadalupian mass extinction. Earth and Planetary Science Letters 196, 113–122.

Zhou, M.-F., Robinson, P.T., Lesher, C.M., Keays, R.R., Zhang, C.J., Malpas, J., 2005. Geochemistry, petrogenesis and metallogenesis of the Panzhihua gabbroic layered intrusion and associated Fe–Ti–V oxide deposits, Sichuan Province, SW China. Journal of Petrology 46, 2253–2280.

Zhou, M.-F., Zhao, J.-H., Qi, L., Su, W., Hu, R., 2006. Zircon U–Pb geochronology and elemental and Sr–Nd isotope geochemistry of Permian mafic rocks in the Funing area, SW China. Contributions to Mineralogy and Petrology 151, 1–19.

Zindler, A., Hart, S.R., 1986. Chemical geodynamics. Annual Review of Earth and Planetary Science 14, 493–571.